Calculation of the properties of the σ meson in a generalized Nambu–Jona-Lasinio model with Lorentz-vector confinement

L. S. Celenza, Xiang-Dong Li, and C. M. Shakin*
Department of Physics and Center for Nuclear Theory, Brooklyn College of the City University of New York, Brooklyn, New York 11210
(Received 4 December 1996)

A recent analysis by Törnqvist and Roos suggests that the σ meson has a mass of 860 MeV with a width of 880 MeV. In this work we calculate the properties of the σ meson using a generalized Nambu–Jona-Lasinio model that includes a model of confinement. We describe, in some detail, how the σ coupling to states in the two-pion continuum may be calculated, when using a Lorentz-vector confining interaction. As part of our work we provide a general procedure for calculating various loop diagrams in Minkowski momentum space for quarks in the presence of the confining interaction. We study the properties of the σ meson by considering t-channel scalar-isoscalar exchange between two quarks. The resulting quark-quark T matrix $t_{qq}(q^2)$ has $\mathrm{Re}\, t_{qq}(q^2)=0$ for $q^2=(0.823\ \mathrm{GeV})^2$. Thus, we have $m_\sigma=0.823$ GeV. However, the coupling of the σ to the two-pion states is so large as to make $|t_{qq}(q^2)|$ a rather smooth function over a broad range of q^2. Therefore, we do not attempt to assign a width for the resonance. [S0556-2813(97)01606-3]

PACS number(s): 24.85.+p, 12.39.Fe, 14.40.Cs

I. INTRODUCTION

It is well known that the SU(2)-flavor version of the Nambu–Jona-Lasinio (NJL) model predicts a scalar-isoscalar meson with mass $m_\sigma^2=(2m_q)^2+m_\pi^2$, where m_q is the constituent quark mass [1]. (We have usually used $m_q=260$ MeV in our work, so that $m_\sigma=540$ MeV.) Since there is no low-mass σ meson in the data tables, it is of interest to consider what happens to the low-mass state predicted by the NJL model as we introduce confinement and coupling to the two-pion continuum. In a recent work Törnqvist and Roos [2], who use a unitary quark model, suggest Breit-Wigner parameters for the σ of $m_\sigma=860$ MeV and $\Gamma_\sigma=880$ MeV. As we will see, our results are generally consistent with the parameters found in Ref. [2].

In this work we wish to show how the NJL model may be generalized to include a model of confinement. We will use Lorentz-vector confinement, rather than the Lorentz-scalar confinement usually used, since the use of vector confinement allows us to maintain the chiral symmetry of the Lagrangian [3]. (That feature is particularly important, if we wish to study the pseudoscalar octet of Goldstone bosons, for example.) We have performed two types of calculations. In Ref. [3] we carried out our calculations in a Euclidean momentum space and were able to do a fully covariant calculation in which we allowed energy transfer via the confining interaction. That work was limited to spacelike values of the momentum $q^2<0$. On the other hand, when we have considered timelike excitations ($q^2>0$), we have neglected energy transfer by the confining interaction. Our method of calculation for timelike q^2 is similar to that used by Gross and Milana [4,5] who assume that the only important singularities to be taken into account when completing integrals over loop four-momenta k^μ are those associated with the quark propagators. (A review of our formalism for the case of Lorentz-scalar confinement may be found in Ref. [6].) In the work reported here, we will be concerned with the timelike region and will neglect energy transfer by the confining interaction. That avoids the necessity of considering singularities associated with that interaction when performing loop integrals.

We will begin our discussion by describing the covariant formalism, which may be used in Euclidean-space calculations. We will then go on to neglect energy transfer. In that approximation, we will provide results for vertex functions of the confining interaction using the formalism presented in Ref. [6].

The Lagrangian of our model is

$$\mathcal{L}=\overline{q(x)}(i\not\partial-m_q^0)q(x)+\frac{G_S}{2}\{[\overline{q(x)}q(x)]^2+[\overline{q(x)}i\gamma_5\boldsymbol{\tau}q(x)]^2\}+\mathcal{L}_{\mathrm{conf}},\tag{1.1}$$

where m_q^0 is the current quark mass. Here, we choose

$$\mathcal{L}_{\mathrm{conf}}=\frac{1}{4}\,\overline{q(x)}\gamma^\mu q(x)V^C(x-y)\overline{q(y)}\gamma_\mu q(y).\tag{1.2}$$

Note that $V^C(r)=\kappa r\exp[-\mu r]$ in the noncovariant formalism, where x and y are at equal time. Since our calculations are made in momentum space, we include a small parameter $\mu=0.030$ GeV to soften the singularities of the Fourier transform of $V^C(r)$. We include the factor $\frac{1}{4}$ in Eq. (1.2) so that the value of κ we quote can be directly compared to the value of κ used in the case of Lorentz-scalar confinement $\kappa\simeq 0.20\ \mathrm{GeV}^2$.

The organization of our work is as follows. In Sec. II we define a vertex function that serves to sum a ''ladder'' of confining interactions. This vertex, when inserted into the quark-antiquark (polarization) loop diagrams, removes the unphysical $q\overline{q}$ unitary cut, so that the loop integral is real. In Sec. III we describe the calculation of polarization diagrams and provide a value for the mass of the σ in the presence of confinement. In Sec. IV we study the coupling of the σ to

*Electronic address: casbc@cunyvm.cuny.edu

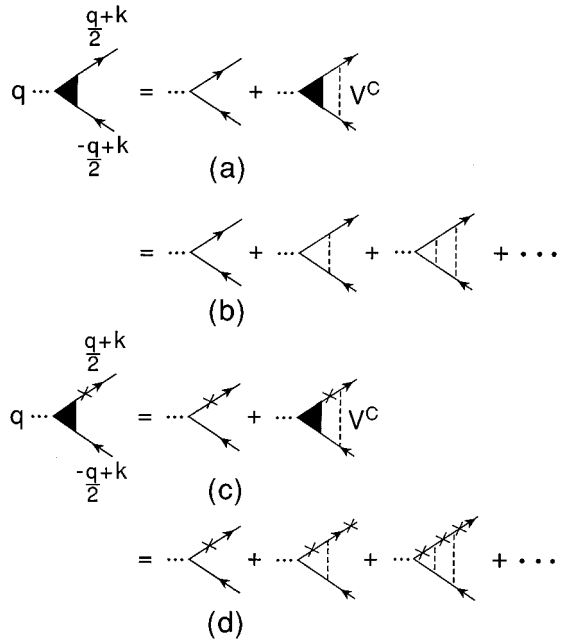

FIG. 1. (a) The diagram represents the equation for the vertex $\overline{\Gamma}_S(q,k)$ that sums a series of confining interactions. These interactions are shown here as dashed lines. (b) A perturbative expansion for $\overline{\Gamma}_S(q,k)$ is shown. (c) The vertex $\Gamma_S^{+-}(q,k)$ is obtained in our analysis when the quark is on its mass shell. (Here the cross denotes a quark on its positive mass shell.) (d) A perturbative expansion for $\Gamma_S^{+-}(q,k)$ is shown. The dashed line introduces a factor $-iV^C(k-k')\gamma^\mu(1)\gamma_\mu(2)/4$ when applying the Feynman rules in the evaluation of the diagrams.

states of two pions and in Sec. V we show how we may calculate the contribution to the σ self-energy due to the coupling to the two-pion continuum. (Again, confinement plays an important role in removing unphysical $q\bar{q}$ cuts in the σ self-energy.) In Sec. V we calculate the imaginary part of the self-energy due to coupling to the two-pion states and go on to calculate the real part using a once-subtracted dispersion relation. (Note that, while the polarization diagrams are of order n_c, the self-energy diagrams considered in Sec. V are of order 1 in the standard counting of color factors.) In Sec. VI, we study the quark-quark T matrix for scalar-isoscalar t-channel exchange and show that the coupling to the two-pion continuum is so large as to leave only slight evidence of the presence of the σ. Section VII contains further discussion and some conclusions.

II. VERTEX FUNCTIONS FOR LORENTZ-VECTOR CONFINEMENT

We have considered (Lorentz) scalar confinement in our earlier work [6–8]. However, we have recently shown that, if one uses Lorentz-vector confinement, one may maintain the chiral symmetry of the Lagrangian, if the current quark mass m_q^0 is 0 [3]. Therefore, we will continue our use of Lorentz-vector confinement in this work. In this section we will consider a scalar-isoscalar vertex function. (We use the notation $S(p)=[\not{p}-m_q+i\epsilon]^{-1}$ for the quark propagator, with m_q being the constituent quark mass.)

With reference to Fig. 1(a), we define a vertex that satisfies the (inhomogeneous) equation [6]

$$\overline{\Gamma}_S(q,k)=1+i\int\frac{d^4k'}{(2\pi)^4}\,\gamma^\mu S(q/2+k')\overline{\Gamma}_S(q,k')\times S(-q/2+k')\gamma_\mu V^C(k-k')/4, \tag{2.1}$$

where, in the covariant formalism,

$$V^C(k-k')=-8\pi\kappa\left\{\frac{1}{[(k-k')^2-\mu^2]^2}+\frac{4\mu^2}{[(k-k')^2-\mu^2]^3}\right\}. \tag{2.2}$$

In the figure, the filled triangular area is the vertex $\overline{\Gamma}_S(q,k)$. In general, one may write

$$\overline{\Gamma}_S(q,k)=a_1(q^2,q\cdot k,k^2)+\hat{\not{k}}a_2(q^2,q\cdot k,k^2)+\not{q}a_3(q^2,q\cdot k,k^2)+2i\sigma_{\mu\nu}q^\mu k^\nu a_4(q,q\cdot k,k^2). \tag{2.3}$$

Here $\hat{k}^\mu=k^\mu-(k\cdot q)q^\mu/q^2$. [In some cases, we will insert a bar over quantities that have Dirac matrix indices; for example, we wrote $\overline{\Gamma}_S(q,k)$ in Eqs. (2.1) and (2.3).] We will not need to consider the general case given in Eq. (2.3), since the functions we calculate will not depend upon the variable $q\cdot k$. (That feature has its origin in our neglect of energy-transfer dependence in the confining interaction.)

When we perform loop integrals in Minkowski space we will first integrate over the timelike component k_0'. In the complex k_0' plane we encounter poles due to the quarks, or antiquarks, going on mass shell. (The contour is usually chosen so that we have poles due to the quarks going on their *positive* mass shell, while the antiquarks go on their *negative* mass shell, when we evaluate polarization diagrams.) In Figs. 1(c) and 1(d) we indicate the nature of the calculation in which the quark is on mass shell. In this case, the relevant vertex will be denoted as $\Gamma_S^{+-}(q,k)$ and, for $\mathbf{q}=0$, we will write $\Gamma_S^{+-}(q^0,|\mathbf{k}|)$. Other vertex functions that appear in our analysis will be denoted as Γ_S^{-+}, Γ_S^{++}, and Γ_S^{--}. We may relate these functions to $\overline{\Gamma}_S(q,k)$ by the following procedure. We first define the standard Dirac projection operators

$$\Lambda^{(+)}(\mathbf{k})=\frac{\not{k}+m_q}{2m_q}, \tag{2.4}$$

with $k^\mu=[E(\mathbf{k}),\mathbf{k}]$, and

$$\Lambda^{(-)}(-\mathbf{k})=\frac{\widetilde{\not{k}}+m_q}{2m_q}, \tag{2.5}$$

with $\widetilde{k}^\mu=[-E(\mathbf{k}),\mathbf{k}]$. Thus, we now define

$$\Lambda^{(+)}(\mathbf{k})\overline{\Gamma}_S\Lambda^{(+)}(\mathbf{k})=\Gamma_S^{++}(q,k)\Lambda^{(+)}(\mathbf{k})\Lambda^{(+)}(\mathbf{k}), \tag{2.6}$$

$$=\Gamma_S^{++}(q,k)\Lambda^{(+)}(\mathbf{k}), \tag{2.7}$$

$$\Lambda^{(-)}(-\mathbf{k})\overline{\Gamma}_S\Lambda^{(-)}(-\mathbf{k})=\Gamma_S^{--}(q,k)\Lambda^{(-)}(-\mathbf{k}), \tag{2.8}$$

$$\Lambda^{(+)}(\mathbf{k})\overline{\Gamma_S}\Lambda^{(-)}(-\mathbf{k})=\Gamma_S^{+-}(q,k)\Lambda^{(+)}(\mathbf{k})\Lambda^{(-)}(-\mathbf{k}), \tag{2.9}$$

and

$$\Lambda^{(-)}(-\mathbf{k})\overline{\Gamma_S}\Lambda^{(+)}(\mathbf{k})=\Gamma_S^{-+}(q,k)\Lambda^{(-)}(-\mathbf{k})\Lambda^{(+)}(\mathbf{k}). \tag{2.10}$$

Usually, we will work in the frame where $\mathbf{q}=0$, so that the various functions we have defined will depend upon q^0 and $|\mathbf{k}|$. In Secs. III and IV, we will see how these functions arise naturally in our Minkowski-space calculations of loop integrals. As we will see, the set of Γ's will be linearly related to the functions a_1, a_2, a_3, and a_4. We may write equations for either set of functions by using standard projection operator and trace techniques, starting with Eq. (2.1). We first present the results for the functions defined in Eq. (2.3). For vector confinement, we find that $a_4=0$ and that

$$a_1(q,-k)=a_1(q,k) \tag{2.11}$$

$$=a_1[q^2,(k\cdot q)^2,k^2], \tag{2.12}$$

$$a_2(q,-k)=a_2(q,k) \tag{2.13}$$

$$=a_2[q^2,(k\cdot q)^2,k^2], \tag{2.14}$$

and

$$a_3(q,-k)=-a_3(q,k) \tag{2.15}$$

$$=(k\cdot q)a_3[q^2,(k\cdot q)^2,k^2]. \tag{2.16}$$

Now, if $V^C(k)$ is independent of k^0, we also have $a_3=0$.

We now neglect energy transfer and find the following equations are obtained for the two remaining functions. Integrating over k_0', and writing $E(k)=[k^2+m_q^2]^{1/2}$, we have

$$a_1(q,k)=1+4\pi\int\frac{k'^2dk'}{(2\pi)^3}\frac{(-8\mathbf{k}'^2)V_0^C(k,k')[a_1(q,k')+m_qa_2(q,k')]}{E(k')\{q_0^2-[2E(k')]^2\}}, \tag{2.17}$$

and

$$a_2(q,k)=-4\pi\int\frac{k'^2dk'}{(2\pi)^3}V_1^C(k,k')\frac{\frac{k'}{k}(4m_q)[a_1(q,k')+m_qa_2(q,k')]}{E(k')\{q_0^2-[2E(k')]^2\}}. \tag{2.18}$$

In these equations $k'=|\mathbf{k}'|$ and $k=|\mathbf{k}|$, and

$$V_l^C(k,k')=\frac{1}{2}\int_{-1}^{1}dxP_l(x)V_C(\mathbf{k}^2+\mathbf{k}'^2-2kk'x)/4. \tag{2.19}$$

The functions $a_1(q,k)$ and $a_2(q,k)$ are related to the functions $\Gamma_S^{+-}(q,k)$, $\Gamma_S^{-+}(q,k)$, etc. We find that $\Gamma_S^{+-}(q,k)=\Gamma_S^{-+}(q,k)$ and $\Gamma_S^{++}(q,k)=\Gamma_S^{--}(q,k)$, with

$$\Gamma_S^{+-}(q,k)=a_1(q,k)+m_qa_2(q,k) \tag{2.20}$$

and

$$\Gamma_S^{++}(q,k)=a_1(q,k)-\frac{\mathbf{k}^2}{m_q}a_2(q,k). \tag{2.21}$$

These last two relations may be obtained by writing $\overline{\Gamma_S}(q,k)=a_1(q,k)+\hat{\mathbf{k}}a_2(q,k)$ and then using the definitions of $\Gamma_S^{+-}(q,k)$, $\Gamma_S^{-+}(q,k)$, etc., given in Eqs. (2.6)–(2.10). Using the equations for $a_1(q,k)$ and $a_2(q,k)$ given above, and Eqs. (2.20) and (2.21), we find that, when $\mathbf{q}=0$,

$$\Gamma^{+-}(q^0,k)=1+4\pi\int\frac{k'^2dk'}{(2\pi)^3}\frac{-8\mathbf{k}'^2}{E(k')}\frac{[V_0^C(k,k')+(m_q^2/2kk')V_1^C(k,k')]}{(q^0)^2-[2E(k')]^2}\Gamma^{+-}(q^0,k'), \tag{2.22}$$

and

$$\Gamma^{++}(q^0,k)=1+4\pi\int\frac{k'^2dk'}{(2\pi)^3}\frac{-8\mathbf{k}'^2}{E(k')}\frac{[V_0^C(k,k')-(k/2k')V_1^C(k,k')]}{(q^0)^2-[2E(k')]^2}\Gamma^{+-}(q^0,k'). \tag{2.23}$$

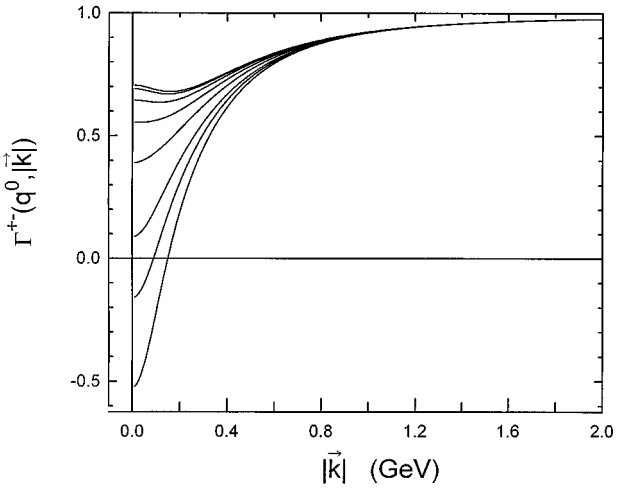

FIG. 2. Values of $\Gamma_S^{+-}(q^0,|\mathbf{k}|)$ are shown. Starting from the uppermost curve and moving downward, the values of q^0 are 0, 0.10, 0.20, 0.30, 0.40, 0.50, 0.55, and 0.60 MeV. For the last two of these curves, $\Gamma_S^{+-}(q^0,|\mathbf{k}_{\rm on}|)=0$. Here $\mathbf{k}_{\rm on}^2=(q_0/2)^2-m_q^2$, $m_q=0.260$ GeV, $\mu=0.030$ GeV, and $\kappa=0.20$ GeV^2.

[We recall that $\Gamma_S^{+-}(q,k)=\Gamma_S^{-+}(q,k)$ and $\Gamma_S^{++}(q,k)=\Gamma_S^{--}(q,k)$, if the k^0 dependence of $V^C(k)$ is ignored. Also note that $\Gamma_S^{++}(q,k)$ may be obtained from $\Gamma_S^{+-}(q,k)$ by using Eq. (2.23).]

Values calculated for $\Gamma_S^{+-}(q,|\mathbf{k}|)$ are given in Fig. 2 for several values of q^0. Note that when *both* the quark and antiquark go on their (positive) mass shell, we have $q^0=2[\mathbf{k}_{\rm on}^2+m_q^2]^{1/2}$ and $\Gamma_S^{+-}(q^0,|\mathbf{k}_{\rm on}|)=0$. This last relation may be used to show how our model of confinement removes unitary cuts that would otherwise arise when the quark and antiquark both go on their positive mass shell [6].

In Fig. 3 we show values obtained for $\Gamma_S^{++}(q^0,|\mathbf{k}|)$. The functions shown in Figs. 2 and 3 will be needed for the calculations described in the following sections.

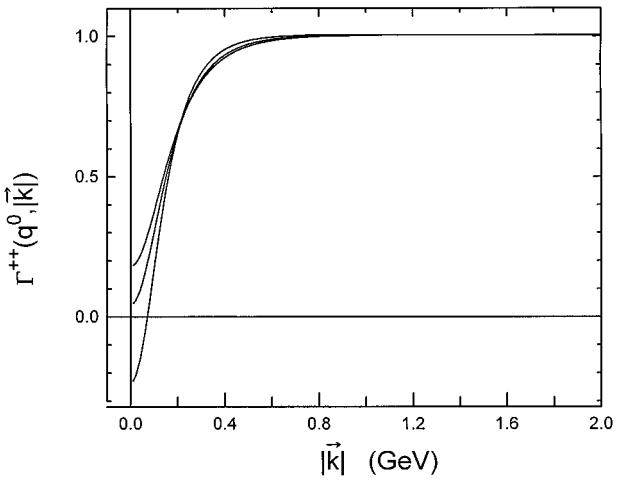

FIG. 3. Values of $\Gamma_S^{++}(q^0,|\mathbf{k}|)$ are shown. Starting with the uppermost curve and moving downward, the values of q^0 are 0, 0.4, and 0.6 GeV. (Here $m_q=0.260$ GeV, $\mu=0.030$ GeV, and $\kappa=0.20$ GeV^2.)

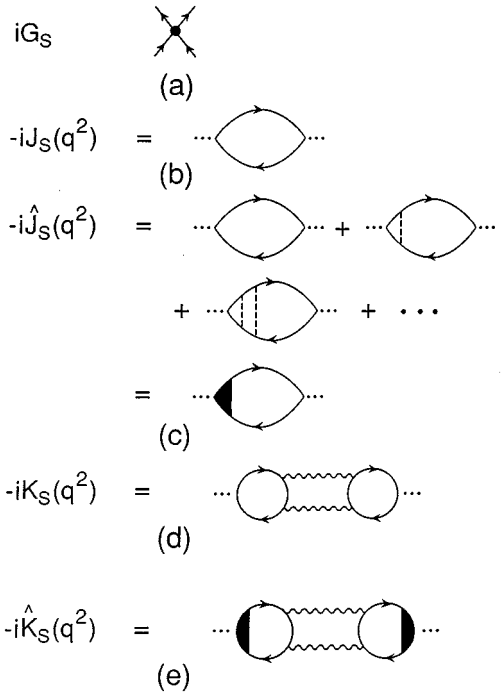

FIG. 4. (a) The zero-range quark interaction of the NJL model is shown. (b) The quark-loop integral in the scalar-isoscalar channel is shown. (c) The quark-loop integral including a series of confining interactions (dashed line) is shown. The filled triangular region denotes the vertex function that serves to sum the ladder of confining interactions. (d) The function $K_S(q^2)$ describes effects of coupling to the two-pion continuum. (e) The function $\hat{K}_S(q^2)$ includes two confinement vertex functions and has a cut for $q^2>4m_\pi^2$.

III. POLARIZATION DIAGRAMS AND THE MASS OF THE σ MESON

It is useful to determine the parameters for the σ meson resonance by studying a quark-quark T matrix evaluated for t-channel scalar-isoscalar exchange processes. (The T matrix we study may be defined even if the quarks are confined.) If we drop reference to Dirac matrices and isospin factors, the polarization diagrams may be summed to yield

$$t_{qq}(q^2)=-\frac{G_S}{1-G_SJ_S(q^2)}, \tag{3.1}$$

where

$$-iJ_S(q^2)=(-1)n_cn_f\ \mathrm{Tr}\int\frac{d^4k}{(2\pi)^4}\,iS\left(\frac{q}{2}+k\right)\times iS\left(-\frac{q}{2}+k\right), \tag{3.2}$$

with $S(p)=[\not{p}-m_q+i\epsilon]^{-1}$. (See Fig. 4.) When we include confinement, we define

$$t_{qq}(q^2)=-\frac{G_S}{1-G_S\hat{J}_S(q^2)}, \tag{3.3}$$

where $\hat{J}_S(q^2)$ is defined in terms of the confining vertex $\overline{\Gamma}_S(q,k)$,

$$-i\hat{J}_S(q^2)=n_c n_f\ \mathrm{Tr}\int\frac{d^4k}{(2\pi)^4}S\left(\frac{q}{2}+k\right)\times\overline{\Gamma}_S(q,k)S\left(-\frac{q}{2}+k\right). \tag{3.4}$$

(See Fig. 5.) As a next step, we use the relation

$$S(k)=\frac{m_q}{E(\mathbf{k})}\left[\frac{\Lambda^{(+)}(\mathbf{k})}{k^0-E(\mathbf{k})+i\epsilon}-\frac{\Lambda^{(-)}(-\mathbf{k})}{k^0+E(\mathbf{k})-i\epsilon}\right] \tag{3.5}$$

in Eq. (3.4). [See Eqs. (2.4) and (2.5).] Therefore, if we work in the frame where $\mathbf{q}=0$,

$$-i\hat{J}_S(q^2)=-n_c n_f\ \mathrm{Tr}\int\frac{d^4k}{(2\pi)^4}\frac{m_q}{E(\mathbf{k})}\left[\frac{\Lambda^{(+)}(\mathbf{k})\overline{\Gamma}_S(q,k)\Lambda^{(-)}(-\mathbf{k})}{[q^0/2+k^0-E(\mathbf{k})+i\epsilon][-(q^0/2)+k^0+E(\mathbf{k})-i\epsilon]}+\frac{\Lambda^{(-)}(-\mathbf{k})\overline{\Gamma}_S(q,k)\Lambda^{(+)}(\mathbf{k})}{[q^0/2+k^0+E(\mathbf{k})-i\epsilon][-(q^0/2)+k^0-E(k)+i\epsilon]}\right], \tag{3.6}$$

where we have kept only the nonzero terms. The first term in Eq. (3.6) introduces $\Gamma_S^{+-}(q,k)$ and the second introduces $\Gamma_S^{-+}(q,k)$. If we evaluate the integral in the lower part of the complex k^0 plane, the first term in Eq. (3.6) leads to the quark being on its positive mass shell $q^0/2+k^0=E(\mathbf{k})$ while the second term leads to the antiquark being on its *negative* mass shell $-q^0/2+k^0=E(\mathbf{k})$. The singularity that would otherwise appear in the result when *both* the quark and the antiquark go on their *positive* mass shell is eliminated by the fact that $\Gamma_S^{+-}(q,k)=0$ at that point [where $q^0=2E(\mathbf{k})$ and $k^0=0$].

In Fig. 6 we show the results of calculations of $J_S(q^2)$ and $\hat{J}_S(q^2)$ for $q^2\geq 0$ [9]. We note that $J_S(q^2)$ is complex for $q^2>4m_q^2$, while $\hat{J}_S(q^2)$ is a real function.

We may determine the mass of the σ meson by solving the equation

$$G_S^{-1}-J_S(m_\sigma^2)=0 \tag{3.7}$$

or the equation

$$G_S^{-1}-\hat{J}_S(m_\sigma^2)=0. \tag{3.8}$$

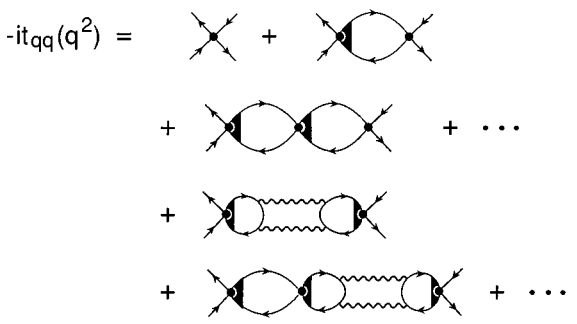

FIG. 5. The quark-quark T matrix, $t_{qq}(q^2)$, is obtained by summing the diagrams shown. The t-channel exchanges are summed by the expression given as Eq. (3.9). In a limited region of q^2 ($-0.25\ \mathrm{GeV}^2<q^2<0$), these effects are well represented by the exchange of an *effective* σ meson with $m_\sigma=540$ MeV.

For Eq. (3.7), we use $G_S=7.91\ \mathrm{GeV}^{-2}$, $m_q=260$ MeV, and a cutoff on the magnitude of $\mathbf{k}$, $|\mathbf{k}|\leq\Lambda_3$. The cutoff is chosen so that our Minkowski-space calculation yields the same value for $J_S(0)$ as a Euclidean space calculation of that quantity made with a cutoff $\Lambda_E=1.0$ GeV. In that manner, we choose $\Lambda_3=0.689$ GeV. [Note that $J_S(0)=0.088\ \mathrm{GeV}^2$.] The upper horizontal line in Fig. 6 corresponding to $G_S^{-1}=(7.91\ \mathrm{GeV}^{-2})^{-1}$ yields a graphical solution of Eq. (3.7) with $m_\sigma=540$ MeV. That value is just above the beginning of the two-quark continuum at $q^2=(2m_q)^2$.

Now, if we solve Eq. (3.8) rather than Eq. (3.7), we see that m_σ takes on a larger value. For example, a graphical solution of Eq. (3.8) appears in Fig. 6, where we now use the

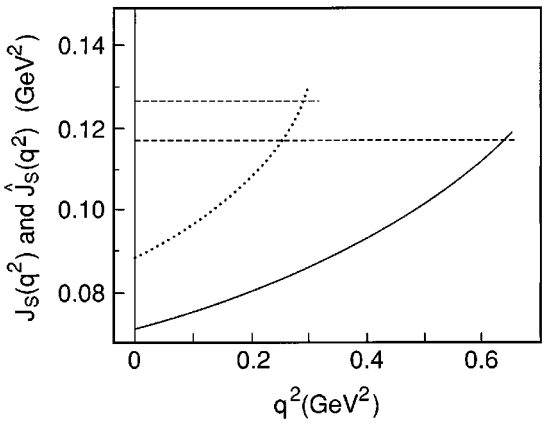

FIG. 6. The figure shows $J_S(q^2)$ and $\hat{J}_S(q^2)$ calculated for $q^2\geq 0$. (We use a cutoff on the three-momenta in the loop integral of $|\mathbf{k}|\leq\Lambda_3$, with $\Lambda_3=0.689$ GeV.) The dotted curve is the result in the absence of confinement and the solid line shows $\hat{J}_S(q^2)$ for Lorentz-vector confinement with $\kappa=0.20\ \mathrm{GeV}^2$. For the dotted curve ($\kappa=0$) we have $G_S=7.91\ \mathrm{GeV}^{-2}$ and for the solid curve ($\kappa=0.20\ \mathrm{GeV}^2$) we have $G_S=8.516\ \mathrm{GeV}^{-2}$. Without confinement we find $m_\sigma=540$ MeV, while, with confinement included, we find $m_\sigma=800$ MeV. The horizontal dashed lines represent G_S^{-1} for the two cases. The intersection of the appropriate dashed line with the dotted or solid lines determines the mass of the σ. Here $J_S(0)=0.088\ \mathrm{GeV}^2$ and $\hat{J}_S(0)=0.0708\ \mathrm{GeV}^2$.

lower horizontal line corresponding to $G_S^{-1}=(8.516\ \mathrm{GeV}^{-2})^{-1}$. [The larger value of G_S used at this point has its origin in our model of confinement [3]. If we write the quark self-energy as $\Sigma(p)=A(p^2)+\not{p}B(p^2)$ and calculate $A(p^2)$ and $B(p^2)$ for the NJL interaction *plus* the confining interaction, we find that $A(p^2)$ varies with p^2, unlike the case of the NJL interaction alone, where $A(p^2)$ is a constant [3]. We also find that $B(p^2)$ is small. We then adjust G_S so that $A(0)$ has the same value m_q that it had when there was no confining interaction. Since the confining interaction behaves as a repulsive interaction, we have to increase G_S to keep $A(0)=m_q$, with the result that $G_S=7.91\ \mathrm{GeV}^{-2}$ is replaced by $G_S=8.516\ \mathrm{GeV}^{-2}$ [3].] Returning to Fig. 6, we see that we have $m_\sigma\simeq 800$ MeV, which is an increase of about 260 MeV above the value of $m_\sigma=540$ MeV found in the absence of confinement.

The quark-quark T matrix can be extended to include diagrams involving $\hat{K}_S(q^2)$, some of which are shown in Fig. 4. In that case, we have

$$t_{qq}(q^2)=-\frac{G_S}{1-G_S[\hat{J}_S(q^2)+\hat{K}_S(q^2)]} \tag{3.9}$$

$$=-\frac{G_S}{1-G_S[\hat{J}_S(q^2)+\mathrm{Re}\ \hat{K}_S(q^2)]-iG_S\ \mathrm{Im}\ \hat{K}_S(q^2)}. \tag{3.10}$$

In the next section we will describe the methods that are used to calculate $\hat{K}_S(q^2)$. The presence of Re $\hat{K}_S(q^2)$ moves the σ mass upward by a small amount. However, introduction of Im $\hat{K}_S(q^2)$ has a rather dramatic effect on the properties of the σ resonance.

IV. COUPLING TO THE TWO-PION CONTINUUM: CALCULATION OF THE AMPLITUDE $q+\bar{q}\to\pi+\pi$ IN THE SCALAR-ISOSCALAR CHANNEL

We will first concentrate on the calculation of Im $\hat{K}_S(q^2)$. Once that calculation is completed, we will use a once-subtracted dispersion relation to calculate Re $\hat{K}_S(q^2)$. Basic to the calculation of Im $\hat{K}_S(q^2)$ is the evaluation of the diagram shown in Fig. 7 for the case of on-mass-shell pions. There, we have $(q/2+\kappa)^2=(q/2-\kappa)^2=m_\pi^2$, so that $q\cdot\kappa=0$.

In the general case, we can define an amplitude

$$\mathcal{F}_S(q,\kappa)=\mathrm{Tr}\ i\int\frac{d^4k}{(2\pi)^4}[S(k-\kappa)\gamma_5 S(q/2+k)\bar{\Gamma}_S(q,k) \times S(-q/2+k)\gamma_5]. \tag{4.1}$$

(See Fig. 7.) Now, if the pions are on-mass-shell, we may define

$$F_1(q^2)=\mathcal{F}_S(q^2,q\cdot\kappa=0,\kappa^2=m_\pi^2-q^2/4). \tag{4.2}$$

(See Fig. 8.) We will also find it useful to introduce

$$F_2(\kappa^2)=\mathcal{F}_S(0,0,\kappa^2). \tag{4.3}$$

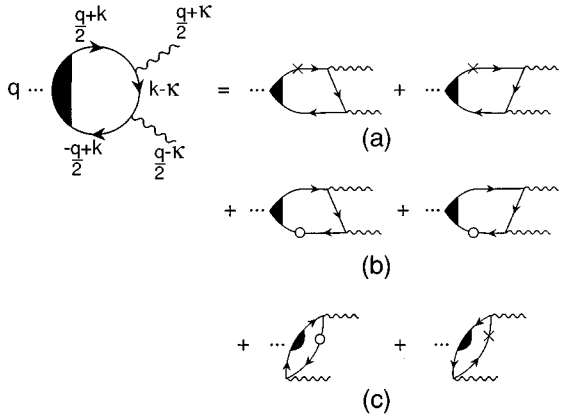

FIG. 7. The diagram corresponding to $\mathcal{F}_S(q^2,q\cdot\kappa,\kappa^2)$ is shown. Here, the wavy lines are pions. (The only factors of i introduced in the definition are those from the propagators.) [See Eq. (4.1).] The diagram is evaluated for $q^2>0$ by first completing the integral over k^0 in the complex k^0 plane. (a) These diagrams introduce the factor $\Gamma_S^{+-}(q,k)$. (b) These diagrams introduce the factor $\Gamma_S^{-+}(q,k)$. (c) The first diagram introduces a factor of $\Gamma_S^{++}(q,k)$, while the second diagram introduces a factor of $\Gamma_S^{--}(q,k)$.

(See Fig. 8.) We will need values of $F_2(\kappa^2)$ when we calculate Re $\hat{K}_S(0)$. (The latter quantity will be needed when we form the once-subtracted dispersion relation.)

We now describe the procedure used to calculate $\mathcal{F}_S(q,\kappa)$ in Minkowski space. First, we use Eq. (3.5) to write each of the three propagators in Eq. (4.1) in terms of $S^{(+)}$ and $S^{(-)}$. That yields eight terms. We now note that, in each of these terms, $\bar{\Gamma}_S(q,k)$ is replaced by $\Gamma_S^{+-}(q,k)$, $\Gamma_S^{-+}(q,k)$, $\Gamma_S^{++}(q,k)$, or $\Gamma_S^{--}(q,k)$, depending upon the location of the $S^{(+)}$ and $S^{(-)}$ factors. [For example, $S^{(+)}(q/2+k)\bar{\Gamma}_S(q,k)S^{(-)}(-q/2+k)$ gives rise to a factor of

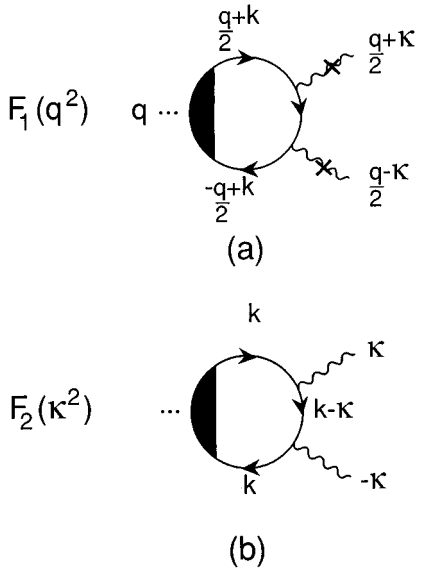

FIG. 8. (a) The diagram that corresponds to $F_1(q^2)$ is shown. Here, the pions are on mass shell, so that $F_1(q^2)=\mathcal{F}_S(q^2,q\cdot\kappa=0,\kappa^2=m_\pi^2-q^2/4)$, where $\mathcal{F}_S(q^2,q\cdot\kappa,\kappa^2)$ is depicted in Fig. 7. $F_1(q^2)$ is needed in the evaluation of Im $\hat{K}_S(q^2)$. (b) The diagram that corresponds to $F_2(\kappa^2)$ is shown, with $F_2(\kappa^2)=\mathcal{F}_S(0,0,\kappa^2)$.

$\Gamma_S^{+-}(q,k)$, etc.] As a next step, we complete the integral over k^0 in the complex k^0 plane. The terms with three $S^{(+)}$ factors, or three $S^{(-)}$ factors, all have their poles in the same half-plane and, therefore, do not contribute to the integral. For the remaining six terms, we choose to complete the k^0 integral either in the upper-half or the lower-half k^0 plane, depending upon where there is only a single pole. The resulting six terms are depicted in Fig. 7. There, a cross on a line denotes a quark on its positive mass shell, while an open circle on a line denotes an antiquark on its *negative* mass shell. For each diagram in Fig. 7(a), one has a factor of $\Gamma_S^{+-}(q,k)$ and for the diagrams of Fig. 7(b), one has a factor of $\Gamma_S^{-+}(q,k)$; however, these two vertex functions are equal, if the interaction does not depend upon energy transfer. Similarly, diagrams of Fig. 7(c) give rise to a factor of $\Gamma_S^{++}(q,k)$, which is equal to the function $\Gamma_S^{--}(q,k)$ arising from the other diagram in Fig. 7(c). The result of these calculations is (for $\mathbf{q}=0$)

$$\mathcal{F}_S(q,\kappa)=4\int\frac{d^3k}{(2\pi)^3}\left\{\frac{(-\mathbf{k}\cdot\boldsymbol{\kappa})}{2m_q^2}\left[\frac{\Gamma_S^{+-}(q^0,k)}{[q^0-2E(\mathbf{k})]\{q^0/2-[E(\mathbf{k})+E(\mathbf{k}-\boldsymbol{\kappa})]\}}+\frac{\Gamma^{-+}(q,k)}{[q^0+2E(\mathbf{k})]\{q^0/2+[E(\mathbf{k})+E(\mathbf{k}-\boldsymbol{\kappa})]\}}\right]\right.$$
$$\left.-\frac{1}{4m_q^2}\frac{[E^2(\mathbf{k})+E(\mathbf{k})E(\mathbf{k}-\boldsymbol{\kappa})-\mathbf{k}\cdot\boldsymbol{\kappa}][\Gamma^{++}(q^0,k)+\Gamma^{--}(q^0,k)]}{[(q^0/2)^2-\{E(\mathbf{k})+E(\mathbf{k}-\boldsymbol{\kappa})]^2\}}\right\},\tag{4.4}$$

where $k=|\mathbf{k}|$. From this function, we may obtain $F_1(q^2)$ and $F_2(\kappa^2)$ as special cases.

In Fig. 9, we show the values we have found for $F_2(\kappa^2)$. Values for $\kappa^2\leqslant 0$ are obtained by evaluating the relevant integral in Euclidean space, where we neglect the effects of confinement. Values for $\kappa^2\geqslant 0$ are obtained using the methods described in this section. If we choose a cutoff for the loop integrals evaluated for $\kappa^2\geqslant 0$ to be $|\mathbf{k}|\leqslant\Lambda_3$, with $\Lambda_3=0.816$ GeV, we find that the value at $\kappa^2=0$ for both calculations is the same. (See Fig. 9.) (Recall that for loop diagrams with *two* quark propagators, the appropriate value of Λ_3 was found to be 0.689 GeV.) We note that confinement effects are small for $q^2\leqslant 0$, so that for $F_2(\kappa^2)=\mathcal{F}_S(0,0,\kappa^2)$, these effects are relatively unimportant.

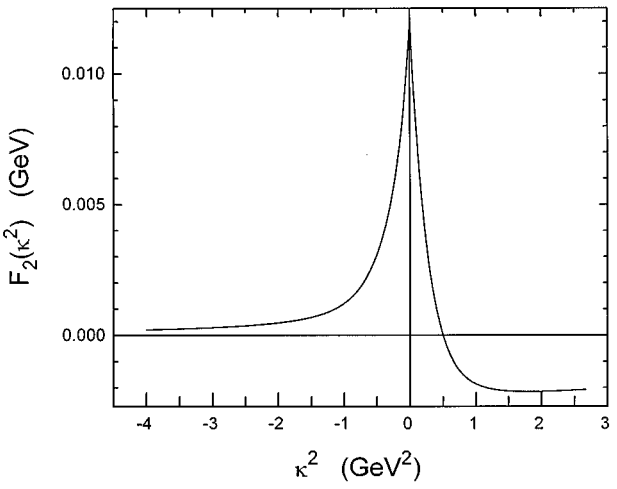

FIG. 9. Values of $F_2(\kappa^2)$ are shown. For $\kappa^2<0$ the calculation is made in a Euclidean momentum space with a cutoff $\Lambda_E=1.0$ GeV. For $\kappa^2>0$, the calculation is made in Minkowski space with a cutoff $|\mathbf{k}|\leqslant\Lambda_3=0.816$ GeV placed upon the integration variable. That cutoff is used for loop integrals having three quark propagators.

V. THE σ SELF-ENERGY INCLUDING COUPLING TO THE TWO-PION CONTINUUM

Once we have calculated $F_1(q^2)$, we may calculate $\mathrm{Im}\,\hat{K}_S(q^2)=(1/2)\,\mathrm{disc}\,\hat{K}_S(q^2)$, where the discontinuity is taken across the two-pion cut that starts at $q^2=4m_\pi^2$. We have

$$\mathrm{disc}\,\hat{K}_S(q^2)=g_{\pi qq}^4 I_f n_c^2 s(-1)\int\frac{d^4\kappa}{(2\pi)^4}[F_1(q^2)]^2$$
$$\times\{-2\pi i\,\delta^{(+)}[(q/2+\kappa)^2-m_\pi^2]\}$$
$$\times\{-2\pi i\,\delta^{(+)}[(q/2-\kappa)^2-m_\pi^2]\},\tag{5.1}$$

where $I_f=12$ is an isospin factor, $n_c^2=9$ is a color factor and $s=2$ is a symmetry factor. Also, the superscript $(+)$ on the δ functions denotes the fact that we choose only the part of the δ function in which the pions are on their positive mass shell.

Now, when $\mathbf{q}=0$,

$$-(2\pi)^2\int\frac{d^4\kappa}{(2\pi)^4}\,\delta^{(+)}\left[\left(\frac{q}{2}+\kappa\right)^2-m_\pi^2\right]$$
$$\times\delta^{(+)}\left[\left(\frac{q}{2}-\kappa\right)^2-m_\pi^2\right]=-\frac{1}{8\pi\omega(\overline{\kappa})}\,\overline{\kappa},\tag{5.2}$$

where $\overline{\kappa}=[(q^0/2)^2-m_\pi^2]^{1/2}$, $\omega(\overline{\kappa})=[\overline{\kappa}^2+m_\pi^2]^{1/2}$, and $q^0=2\omega(\overline{\kappa})$. Thus,

$$\mathrm{Im}\,\hat{K}_S(q^2)=\frac{1}{2}\,g_{\pi qq}^4 I_f n_c^2 s[F_1(q^2)]^2\left(\frac{\overline{\kappa}}{8\pi\omega(\overline{\kappa})}\right)$$
$$\times\theta(q^2-4m_\pi^2).\tag{5.3}$$

Values of $\mathrm{Im}\,\hat{K}_S(q^2)$, calculated using Eq. (5.3), are given in Fig. 10 for the case $g_{\pi qq}=2.68$. That value for $g_{\pi qq}$ was first obtained in Ref. [10]. A simple estimate of $g_{\pi qq}$ may be found by working in the chiral limit, $m_q^0=0$, and evaluating

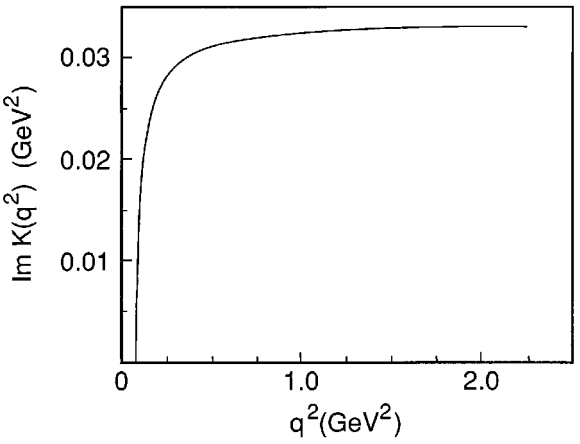

FIG. 10. Values of $\mathrm{Im}\,\hat{K}_S(q^2)$ are shown. The calculation is made using the method outlined in Ref. [5]. Here we use $\kappa = 0.20$ GeV^2, $g_{\pi qq}=2.58$, and Lorentz-vector confinement. We also have $m_q = 260$ MeV and a cutoff on the three-momenta $|\mathbf{k}| \leqslant \Lambda_3$, with $\Lambda_3 = 0.816$ GeV. (Note that the result is quite insensitive to the model of confinement used.) To obtain the values for $g_{\pi qq}=2.68$, we need to multiply the values in the figure by $(2.68/2.58)^4 = 1.16$.

$$\frac{g^2_{\sigma qq}(0)}{m^2_\sigma} = \frac{G_S}{1 - G_S \hat{J}_S(0)}. \tag{5.4}$$

Then, one may put $g_{\pi qq} = g_{\sigma qq}$. A more accurate value is found by using the relation

$$g^{-2}_{\pi qq}(m^2_\pi) = \left.\frac{\partial J_P(q^2)}{\partial q^2}\right|_{q^2 = m^2_\pi}, \tag{5.5}$$

where $J_P(q^2)$ is the value of the (polarization) loop integral in the pseudoscalar channel.

Once we have calculated $\mathrm{Im}\,\hat{K}_S(q^2)$, we can obtain $\mathrm{Re}\,\hat{K}_S(q^2)$ by means of a once-subtracted dispersion relation

$$\mathrm{Re}\,\hat{K}_S(q^2) = \hat{K}_S(0) - \frac{\mathrm{P}}{\pi} q^2 \int_{4m^2_\pi} ds\, \frac{\mathrm{Im}\,\hat{K}_S(s)}{s(q^2 - s)}. \tag{5.6}$$

As a next step, we need to calculate $\hat{K}_S(0)$, which may be obtained in terms of $F_2(\kappa^2)$. We have

$$\hat{K}_S(0) = g^4_{\pi qq} I_f n_c^2 si \int \frac{d^4\kappa}{(2\pi)^4} \left(\frac{i}{\kappa^2 - m^2_\pi}\right)^2 [F_2(\kappa^2)]^2. \tag{5.7}$$

This integral may be completed by going over to a Euclidean momentum space. Using the values of $F_2(\kappa^2)$ given in the last section, and again using $g_{\pi qq}=2.68$, we find $\hat{K}_S(0) = 0.0108$ GeV^2. Using that value in Eq. (5.3), we find the values of $\mathrm{Re}\,\hat{K}_S(q^2)$ shown in Fig. 11. (The sharp peak in that function is due to the rapid opening of the two-pion channel at $q^2 = 4m^2_\pi$.)

Note that, if we write

$$\mathrm{Im}\,\hat{K}_S(q^2) = \left(1 - \frac{4m^2_\pi}{q^2}\right)^{1/2} K_0\, \theta(q^2 - 4m^2_\pi), \tag{5.8}$$

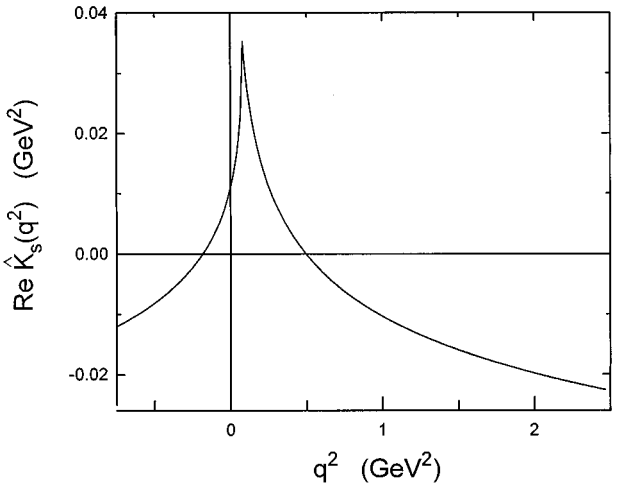

FIG. 11. Values of $\mathrm{Re}\,\hat{K}_S(q^2)$ obtained from the once-subtracted dispersion relation of Eq. (5.6) are shown. Here, $g_{\pi qq}=2.68$ was used in the calculation of $\mathrm{Im}\,\hat{K}_S(q^2)$. [See Fig. 10, which shows $\mathrm{Im}\,\hat{K}_S(q^2)$ calculated for $g_{\pi qq}=2.58$.]

with K_0 a constant, we have an accurate approximation for $\mathrm{Im}\,\hat{K}_S(q^2)$. We can then complete the integrals in Eq. (5.6) with the result, for $q^2 > 4m^2_\pi$,

$$\mathrm{Re}\,\hat{K}_S(q^2) = \hat{K}_S(0) + \frac{2K_0}{\pi}\left[1 + \frac{x}{2}\ln\left(\frac{1-x}{1+x}\right)\right], \tag{5.9}$$

where

$$x \equiv \left[1 - \frac{4m^2_\pi}{q^2}\right]^{1/2}. \tag{5.10}$$

For $0 < q^2 < 4m^2_\pi$, we have

$$\mathrm{Re}\,\hat{K}_S(q^2) = \hat{K}_S(0) + \frac{2K_0}{\pi}\left[1 - \left|1 - \frac{4m^2_\pi}{q^2}\right|^{1/2} \times \tan^{-1}\left(\frac{q^2}{|q^2 - 4m^2_\pi|}\right)^{1/2}\right]. \tag{5.11}$$

We now have enough information to calculate $\hat{J}_S(q^2) + \mathrm{Re}\,\hat{K}_S(q^2)$. That quantity is shown in Fig. 12.

VI. CALCULATION OF THE QUARK-QUARK SCATTERING AMPLITUDE FOR *t*-CHANNEL SCALAR-ISOSCALAR EXCHANGE

Since we now have values of $\hat{J}_S(q^2) + \mathrm{Re}\,\hat{K}_S(q^2)$ and $\mathrm{Im}\,\hat{K}_S(q^2)$, we are able to obtain $t_{qq}(q^2)$ that was defined in Eqs. (3.9) and (3.10). In Fig. 13 we show $\mathrm{Re}\,t_{qq}(q^2)$ as a solid line and $\mathrm{Im}\,t_{qq}(q^2)$ as a dotted line. Note that $\mathrm{Re}\,t_{qq}(q^2)$ has a zero at $q^2 = m^2_\sigma$, corresponding to the equation

$$G_S^{-1} - [J_S(m^2_\sigma) + \mathrm{Re}\,\hat{K}_S(m^2_\sigma)] = 0. \tag{6.1}$$

The very large negative value for $q^2 \simeq 4m^2_\pi$ seen for $\mathrm{Re}\,t_{qq}(q^2)$ has its origin in the opening of the two-pion channel at that energy.

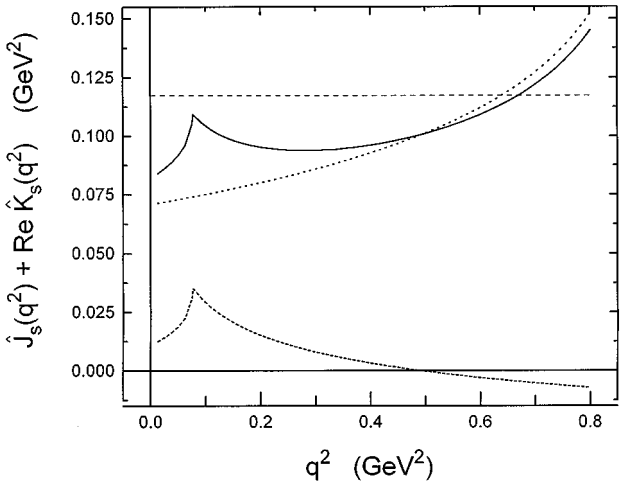

FIG. 12. The dashed line shows Re $\hat{K}_S(q^2)$. (See Fig. 11.) The dotted line shows the values of $\hat{J}_S(q^2)$ calculated in Minkowski space, with $m_q=260$ MeV and a cutoff $\Lambda_3=0.689$ GeV. The solid line shows $\hat{J}_S(q^2)+\mathrm{Re}\,\hat{K}_S(q^2)$. The dot-dashed line shows the value of $G_S^{-1}=(1/8.516)$ GeV^2. The intersection of the solid line with the dot-dashed line depicts the solution of the equation $G_S^{-1}-[\hat{J}_S(m_\sigma^2)+\mathrm{Re}\,\hat{K}_S(m_\sigma^2)]=0$. We find $m_\sigma=823$ MeV. (For these calculations $\kappa=0.20$ GeV^2 and $\mu=0.030$ GeV.)

In Fig. 14 we show values of $|t_{qq}(q^2)|^2$. Again, the large peak in that quantity reflects the opening of the two-pion channel at $q^2=4m_\pi^2$. It may be seen that there is little evidence for the presence of a resonance centered around $q^2=m_\sigma^2$ due to the strong coupling to the two-pion continuum. To investigate this point further, we show $|t_{qq}(q^2)|^2$ in Fig. 15 using an expanded scale. One may note a small enhancement centered around $q^2\sim 0.67$ GeV^2 that could be interpreted as a residual effect due to the presence of the σ resonance.

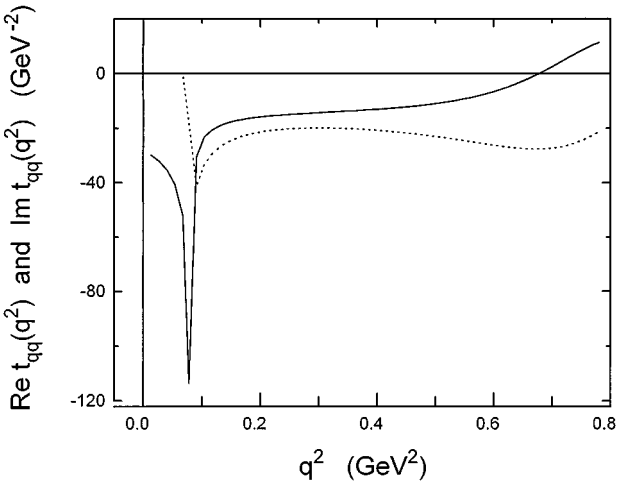

FIG. 13. Values of $\hat{J}_S(q^2)+\mathrm{Re}\,\hat{K}_S(q^2)$ (see Fig. 12) and Im $\hat{K}_S(q^2)$ (see Fig. 10) are used to form Re $t_{qq}(q^2)$, shown as a solid line, and Im $t_{qq}(q^2)$, shown as a dotted line. [The large dip in the value of Re $t_{qq}(q^2)$ corresponds to the opening of the two-pion continuum at $q^2=4m_\pi^2$.]

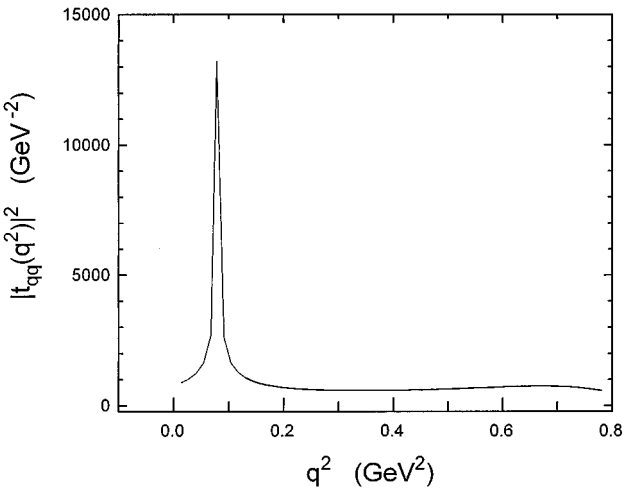

FIG. 14. Values of $|t_{qq}(q^2)|^2$ are shown. [See Fig. 13 for Re $t_{qq}(q^2)$ and Im $t_{qq}(q^2)$.]

VII. DISCUSSION

In a previous work [9] we have studied the quark-quark T matrix $t_{qq}(q^2)$ for spacelike values of q^2. In the present work we have extended our considerations to study $t_{qq}(q^2)$ in the timelike region. For $q^2\leqslant 0$, and for $-q^2$ not too large, the approximation

$$t_{qq}(q^2)=\frac{g_{\sigma qq}^2}{q^2-m_\sigma^2} \tag{7.1}$$

was found to be quite accurate, if $m_\sigma=540$ MeV and $g_{\sigma qq}=3.05$ [9]. In the present work, we may find $g_{\sigma qq}^2$ by writing

$$\frac{G_S}{1-G_S[\hat{J}_S(0)+\hat{K}_S(0)]}=\frac{g_{\sigma qq}^2}{m_\sigma^2}, \tag{7.2}$$

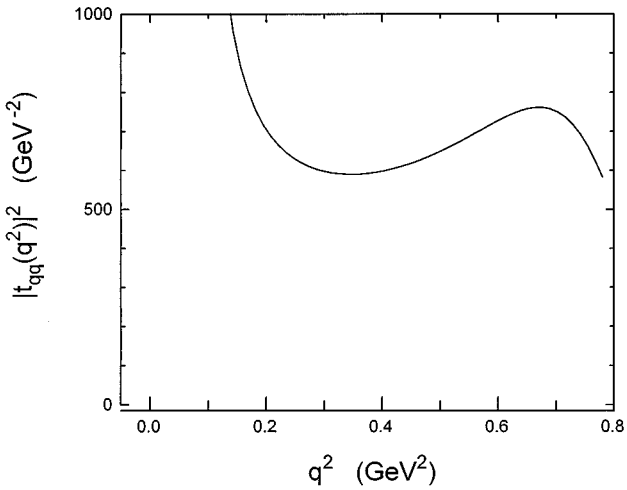

FIG. 15. Values of $|t_{qq}(q^2)|^2$ are shown in an expanded scale relative to that used in Fig. 14. The enhanced values for $q^2\sim 0.7$ GeV^2 correspond to the zero of Re $t_{qq}(q^2)$ at $q^2=0.677$ GeV^2. (See Fig. 13.)

where $m_\sigma = 0.540$ GeV. For the parameters developed here, $\hat{J}_S(0) = 0.0708$ GeV^2, $\hat{K}_S(0) = 0.0108$ GeV^2, and $G_S = 8.516$ GeV^{-2}, we find $g_{\sigma qq} = 2.86$, if $m_\sigma = 0.540$ GeV. Thus, $t_{qq}(0) = -g^2_{\sigma qq}/m^2_\sigma = -28.0$ GeV^{-2}. (See Fig. 13.)

Equation (7.1) is useful in the spacelike domain if $-q^2 < 0.25$ GeV^2. For an accurate representation beyond that region, one may write

$$t_{qq}(q^2) = \frac{g^2_{\sigma qq}(q^2)}{q^2 - m^2_\sigma}. \tag{7.3}$$

[Equation (7.3) may be used to define $g_{\sigma qq}(q^2)$.] Note that, although Eq. (7.1) represents the T matrix for a limited region of spacelike values of q^2, there is no low-mass scalar-isoscalar state in the timelike region. However, for calculation of the NN force, or for the study of nuclear matter, the momenta of the exchanged mesons are spacelike. Therefore, we may conclude that, if one restricts oneself to the description of mesons with spacelike momenta, the introduction of a σ ''meson'' with $m_\sigma = 540$ MeV is quite a good approximation. We have also seen that the use of a low-mass σ for *spacelike* q^2 *is not in contradiction to the fact that such a meson has not been seen*. Also, in the present study, we have found little direct evidence for a more massive resonance in the timelike region because of the very strong coupling to the two-pion continuum of the scalar-isoscalar state. On the other hand, the 0 of the real part of the T matrix, found using Eq. (6.1), does define a mass that the σ would have, if Im $\hat{K}_S(q^2)$ were neglected. We have also seen that there is a large peak in $|t_{qq}(q^2)|$ at $q^2 \sim 4m^2_\pi$. We do not know whether such an effect could be observed in some experiment. However, we again note that the T matrix for spacelike q^2 is not influenced by the peak at $q^2 \sim 4m^2_\pi$. For nuclear physics problems that are of interest to us, the mesons exchanged between nucleons (or between quarks) are spacelike, with Eq. (7.1) providing an accurate representation of the dynamics.

ACKNOWLEDGMENT

This work was supported in part by a grant from the National Science Foundation and by PSC-CUNY.

[1] For reviews of the NJL model, see U. Vogl and W. Weise, Prog. Part. Nucl. Phys. **27**, 1995 (1991); S. P. Klevansky, Rev. Mod. Phys. **64**, 649 (1992); T. Hatsuda and T. Kunihiro, Phys. Rep. **247**, 223 (1994).

[2] N. A. Törnqvist and M. Roos, Phys. Rev. Lett. **76**, 1575 (1996).

[3] L. S. Celenza, Xiang-Dong Li, and C. M. Shakin, Phys. Rev. C **55**, 3987 (1997).

[4] F. Gross and J. Milana, Phys. Rev. D **43**, 2401 (1991).

[5] F. Gross and J. Milana, Phys. Rev. D **45**, 969 (1992).

[6] L. S. Celenza, C. M. Shakin, Wei-Dong Sun, J. Szweda, and Xiquan Zhu, Phys. Rev. D **51**, 3636 (1995).

[7] L. S. Celenza, C. M. Shakin, and J. Szweda, Int. J. Mod. Phys. E **2**, 437 (1993).

[8] L. S. Celenza, C. M. Shakin, Wei-Dong Sun, J. Szweda, and Xiquan Zhu, Int. J. Mod. Phys. E **2**, 603 (1993).

[9] L. S. Celenza, Xiang-Dong Li, C. M. Shakin, and Wei-Dong Sun, Brooklyn College Report No. BCCNT 96/111/258, 1996 (unpublished).

[10] Nan-Wei Cao, C. M. Shakin, and Wei-Dong Sun, Phys. Rev. C **46**, 2535 (1992).